JOURNAL OF MATERIALS SCIENCE: MATERIALS IN MEDICINE 6 (1995) 581–589

The effect of exposure to biological fluids on the spallation resistance of diamond-like carbon coatings on metallic substrates

L. CHANDRA* M. ALLEN‡, R. BUTTER§, N.RUSHTON‡, A.H. LETTINGTON§, T.W. CLYNE*
*Department of Materials Science and Metallurgy, Pembroke Street, Cambridge CB2 3QZ, UK
‡Orthopaedic Research Unit, Addenbrooke's Hospital, Hills Road, Cambridge, CB2 2QQ, UK
§J.J. Thomson Physical Laboratory, University of Reading, PO Box 220, Reading, RG6 2AF, UK

Diamond-like carbon (DLC) films have been deposited by RF plasma-assisted glow discharge CVD on AISI 304 stainless steel and Ti–6Al–4V substrates. A substrate plastic straining technique (to measure the strength and adhesion of the coating) and erosion testing (to measure its durability) have been used, before and after exposure to various fluids (distilled water, phosphate buffered saline solution (PBS) and bovine serum). The films on both substrates had excellent adhesion before exposure to the fluid, being slightly higher for those on Ti substrates. PBS solution affected the adhesion adversely, whereas distilled water and serum had no apparent effect. Fourier transform infrared (FTIR) and Raman spectroscopic studies revealed that there were no changes in the atomic structure of the coatings during exposure. X-ray photoelectron spectroscopy (XPS) measurements indicated that PBS tends to penetrate through perforations in the film and attack the thin transition layer of graded Si/C composition between the a: Si–H layer and the DLC coating. An increase in exposure temperature increased the population of defects in samples exposed to PBS. Coatings on Ti exhibited similar characteristics, but were considerably more resistant to damage. This may be due to a lower incidence of defects and perforations in these films.

1. Introduction

Use of prosthetic implants is increasing rapidly. Hip replacements alone now exceed 200 000 annually in the USA, with similar numbers in Europe [1]. Failures of such joints are, however, still common, with average lifetimes for artificial hips of around 10 years for patients over 70 years of age. Materials suited for prostheses are those which have good bio-tolerance and can withstand cyclic loading in the presence of body fluids. Implants are commonly made of cobalt–chromium alloy (Co–30Cr–3Mo), 318 titanium (Ti–6Al–4V) or 304 stainless steel (Fe–18Cr–8Ni), with ball sockets usually made of a polymer such as ultra high molecular weight polyethylene. Diamond-like carbon (DLC) coatings, because of their mechanical and wear resistant properties [2–4], low coefficient of friction [4] and biocompatibility [5, 6], are of interest as a protective coating in joint replacements [7, 8]. Several research groups are investigating DLC films for biomedical applications [1, 9, 10].

For DLC films to be used in this way, the effect of exposure to biological fluids must be investigated, since this may affect the adhesion of the film to the implant. Furthermore, the biocompatibility of damaged coatings may differ from that of intact coatings. It is well established that the biological response to particulate wear debris can be very different to that of the corresponding bulk material [11–13]. If adhesion of the DLC coatings is adversely affected by exposure to body fluids, small particles of DLC may be released into the joint and could stimulate an inflammatory response.

In the present paper, the effect of various fluids on the adhesion of DLC coatings is investigated experimentally, building on earlier preliminary work [14].

2. Experimental procedure

2.1. Coating production

Diamond-like carbon films, with an amorphous silicon-rich intermediate layer [15, 16] to improve adhesion, were deposited on stainless steel (AISI 304) and Ti–6Al–4V substrates, using a standard RF (13.56 MHz) glow discharge chemical vapour deposition (CVD) technique. Plate specimens of 30 mm × 10 mm × 1 mm were sputter cleaned with argon prior to deposition of a thin (60–70 nm) layer of amorphous hydrogenated silicon (a-Si: H), using silane (SiH_4) as the source gas. A progressive switch to butane (C_4H_{10}) as the source gas produced an interface of varying

0957–4530

TABLE I Conditions used to sputter clean, deposit an a–Si–H intermediate layer and deposit DLC films on metallic substrates by a glow discharge technique

Parameter	Ar sputtering	a-Si:H inter-layer	DLC
Chamber pressure (Pa)	1450	330	400
Substrate temperature (°C)	(See Section 2.1)	180–200	180–200
Bias voltage (kV)	1.2	1.0	0.95
Argon gas flow rate (cm^3/min)	30	–	–
Silane gas flow rate (cm^3/min)	–	10	–
Butane gas flow rate (cm^3/min)	–	–	10
Film thickness (μm)	–	~ 0.075	Steel-1.1 μm Titanium-1.2 μm
Time (min)	10	6	75

TABLE II Specimen codes and exposure conditions

Code	Substrate	Exposure temperature (°C)	Exposure fluid	Exposure time (weeks)
St-AsP	Steel	-	-	As-prepared
St37PBS1	Steel	37	PBS	1
St60PBS1	Steel	60	PBS	1
St37PBS4	Steel	37	PBS	4
St60PBS4	Steel	60	PBS	4
St37SER4	Steel	37	40% Serum in PBS	4
St37WAT4	Steel	37	Distillled water	4
Ti–AsP	Ti–6–4	-	-	As-prepared
Ti37PBS1	Ti–6–4	37	PBS	1
Ti37PBS4	Ti–6–4	37	PBS	4
Ti37SER4	Ti–6–4	37	40% Serum in PBS	4
Ti37WAT4	Ti–6–4	37	Distilled water	4

stoichiometry (< 15 nm thick) between the a-Si: H and a-C: H (the DLC film). The substrate temperature during argon sputtering increased from room temperature to around 180–200 °C, which was maintained during deposition. The deposition conditions are shown in Table. I.

2.2. Environmental exposure testing

The DLC-coated substrates were sterilized with ethylene oxide, prior to testing *in vitro*. Samples were immersed in a fluid in a four-well polystyrene plate. The fluids used were distilled water (WAT), phosphate-buffered saline (PBS) solution (standard isotonic physiological buffer solution) and 40% bovine serum in PBS (SER). The exposure was carried out under standard tissue culture conditions in an incubator maintained at 37 °C, with a humidified atmosphere containing 5% carbon dioxide. The samples were examined after periods of 1 week and 4 weeks. At the end of the test period, samples were washed in Trypsin-EDTA – to remove any protein – and then in detergent (1% Triton X-100 in PBS) – to remove any organic debris. Samples were also exposed to PBS at 60 °C. Table II gives details of the conditions and corresponding specimen codes.

2.3. Surface roughness measurement

The surface roughness of coated and uncoated substrates was determined by using a Dektak^{3}ST profilometer with a horizontal resolution of 10 nm and a vertical resolution of 0.1 nm. The roughness data were acquired under a constant stylus force of 40 mg, with a scan length of 5 mm. At least two measurements were made on each sample.

2.4. FTIR and Raman spectroscopy

Reflection spectra were acquired at 26.5° incidence in the 4000–400 cm^{-1} region, using a Mattson Research Series Fourier Transform Infrared (FTIR) spectrometer, operating at 2 cm^{-1} resolution. This technique gives information about the nature of the interatomic bonding. The presence of thin film interference fringes allowed the calculation of refractive indices of the

DLC coatings, using the following relationship

$$2nd = \frac{1}{\Delta K} \quad (1)$$

where n is the refractive index, d is the film thickness and ΔK is the difference in wave number of successive fringe maxima or minima.

A Spectra Physics Series 2000 argon ion laser operating at 514.54 nm and 0.4 W output power was used as an excitation source for Raman spectra. Data were acquired at room temperature (300 K), in the spectral range 19 100–15 000 cm^{-1} (corresponding to a wave number shift of 335 cm^{-1} to 4435 cm^{-1}). A Spex 1401 double spectrometer, with scan speed 10 $cm^{-1} s^{-1}$ and integration time 1 s was used. The spectrometer slit width was set at 1.2 mm, which was sufficiently wide to allow adequate signal strength. Several scans of each sample were made, and the spectra were averaged to improve the signal-to-noise ratio. A subtraction of a fraction (typically 0.1) of the appropriate uncoated metal spectrum from the sample spectrum was performed, followed by a baseline correction, to eliminate the contributions from laser plasma lines.

2.5. XPS spectroscopy

X-ray photoelectron spectroscopy (XPS) data from the coated samples before and after exposure to fluids were obtained using an AEI Electron Spectrometer model ESCA-ES-200. Specimens were irradiated from an Al K_α source ($h\nu$ = 1486.6 eV) under a vacuum of 10^{-6} Pa. XPS spectra were obtained in the analyser constant energy mode, with a pass energy of 20 eV. (The pass energy, which is the retarding energy used to decelerate the photo-electrons before reaching the analyser, affects the energy resolution.) First, a wide scan between 1300 eV to 0 eV was carried out at intervals of 1 eV. Then, a few narrow scans (over the energy ranges corresponding to oxygen, carbon and silicon) were carried out to obtain more detailed information. A total of 50 such narrow scans for each element were carried out with intervals of 0.1 eV. The escape depths of these photoelectrons are of the order of a few nanometres, so that the technique samples only a very thin surface layer.

2.6. Adhesion measurement by substrate plastic straining

A substrate plastic straining technique [17, 18] was used to characterize the adhesion of the films before and after exposure. The substrate was subjected to an increasing tensile plastic strain, causing the film to crack and break up into segments. A simple variant of the shear lag model was used in analysing the data.

Incremental strains were applied to the "dog-bone" specimens with a constant crosshead displacement rate of 1 mm min^{-1} (corresponding to a strain rate of approximately 10^{-3} s^{-1}). The details of the testing procedure used and its limitations are given elsewhere [17]. In making crack spacing distribution assessments, about 200 measurements were taken in each case. These were used to establish the average saturation crack spacing, $\bar{S}_\infty$. Measurement of the crack initiation strain by test interruption tends to give an overestimate, because of the difficulty in detecting cracks which close after removal of the applied load. Crack initiation strains were therefore corrected, assuming a level of overestimation established earlier [17].

2.7. Erosion testing

Erosive wear of the DLC coated substrates was examined using a technique developed by Hutchings and Shipway [19–21]. This involves measurement of the diameter of the circular wear scar formed by a stream of impinging particles. Field *et al.* [22, 23] have used a similar method to study the erosion of diamond films by high speed water droplets.

The critical dose of particles (cumulative mass per unit area) striking the coating, Q_c, just sufficient to cause penetration to the substrate, either by progressive wear or by debonding of the coating, was determined before and after exposure of samples to fluids. The erodent material used in the work was angular silica sand sieved to particle sizes between 125 and 150 μm. The particle density was 2.60 ± 0.50 $Mg m^{-3}$. A feed rate of 1 g min^{-1} was maintained at a suction pressure of 5000 Pa. The particle velocity was 30 ± 0.5 m s^{-1}. Further details of the technique are given elsewhere [19–21]. The value of Q_c provides a measure of the durability of the coating.

3. Results and discussion

3.1. Appearance of coatings

3.1.1. Coatings on steel substrates

While the coatings exposed to distilled water showed no significant difference in surface morphology from the as-prepared samples, those exposed to PBS and bovine serum showed varying degrees of damage. Micrographs such as Fig. 1a suggest that the film was damaged extensively when exposed to PBS solution for 4 weeks. The coatings exposed to bovine serum were also damaged in some localized areas (Fig. 1b). The coatings exposed to PBS and serum for 1 week also showed significant damage, indicating that most of the damage occurs within the first few days of exposure.

The coatings exposed to PBS at 60 °C showed even greater levels of damage, as shown in Fig. 2a. Each white spot on this micrograph is a damaged area, as highlighted in Fig. 2b. There are at least three possible reasons for this enhancement of damage at higher temperature. First, differential thermal expansion ($\alpha_{subs} > \alpha_{coat}$) on heating will make the residual stress in the coating more tensile (i.e. less compressive), presumably favouring the opening of pores and cracks. Second, at higher temperature any diffusion-controlled process, such as a chemical reaction or capillarity-driven diffusive penetration of liquid, will occur at a faster rate. Finally, the surface tension of the liquid, opposing its entry into fine perforations in the film, will be reduced at higher temperature.

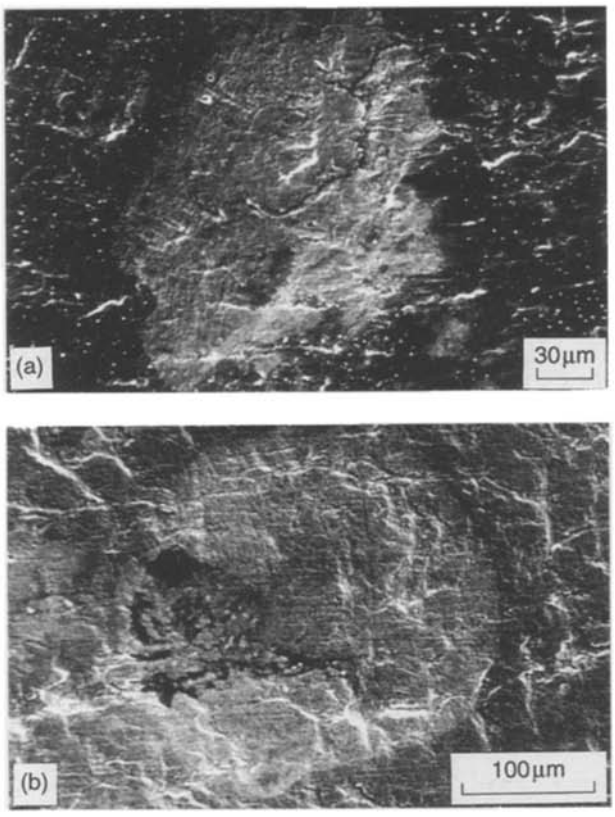

Figure 1 Scanning electron micrographs of (a) specimen St37PBS4 and (b) specimen St37SER4.

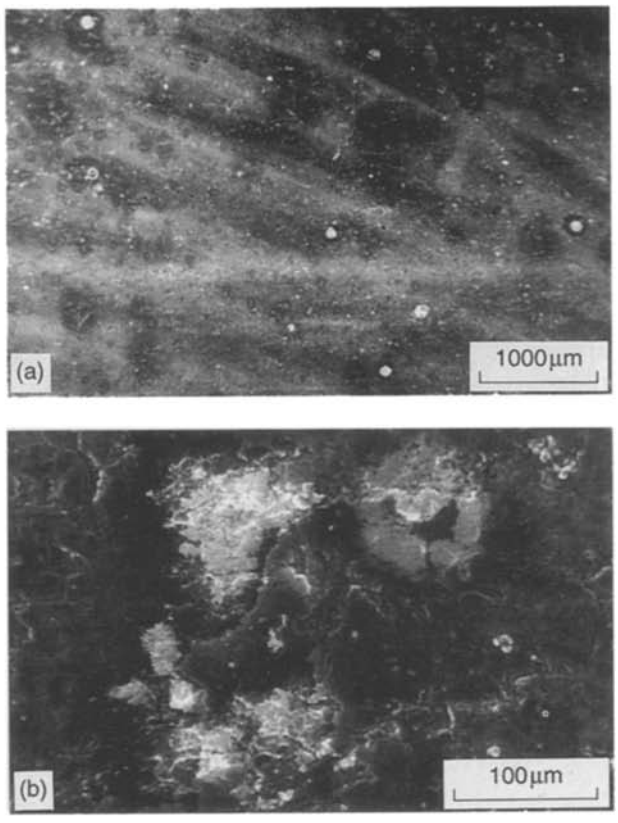

Figure 2 Scanning electron micrographs of specimen St60PBS4 at (a) low and (b) high magnifications.

The population of damage sites (rather than their size) appeared to increase at higher temperature. This suggests that a residual stress-driven effect may be likely, since this will tend to affect the nucleation of defects rather than their growth. However, the same might be expected of the surface tension effect and more evidence is needed in order to draw any firm conclusions.

Damage appears to develop in two stages. At first, liquid seeps through surface defects (perforations and cracks) and attacks the interface, leading to debonding and cracking of the film. This is shown in Fig. 3a. Second, the debonded coating delaminates, leaving behind a crater on the film surface (Fig. 3b). It seems likely that it is the a-Si: H/a–C: H interface which is prone to attack by PBS solution (Section 3.2).

3.1.2. Coatings on titanium substrates

In contrast to the steel case, the coatings on Ti–6–4 substrates did not show any obvious damage to the coating when exposed to either of the above fluids. SEM examination of as-prepared DLC-coated Ti–6–4 revealed a lower incidence of defects in the coating, with a smoother surface and a finer grain size, when compared with those on steel substrates (Fig. 4). This could in turn be attributed to differences in initial substrate surface topography, since the titanium substrate was smoother than the steel substrate (Table III). Thus the reduced damage to the coating on Ti–6–4 after exposure may have arisen because the incidence of initial defects in the coating was lower.

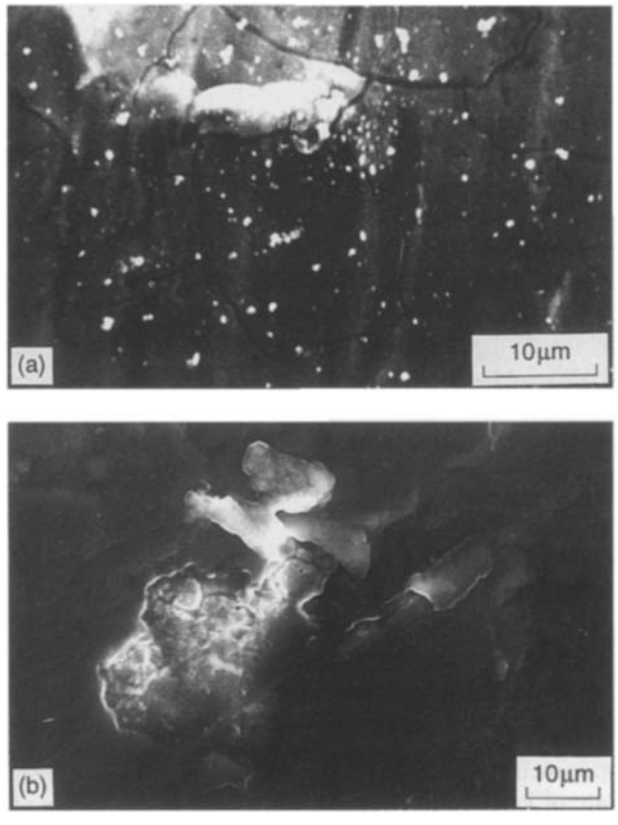

Figure 3 Scanning electron micrographs of specimen (a) St37PBS1, showing cracking of the film after exposure to PBS for 1 week, and (b) St37PBS4, showing delamination of the coating after exposure to PBS for 4 weeks.

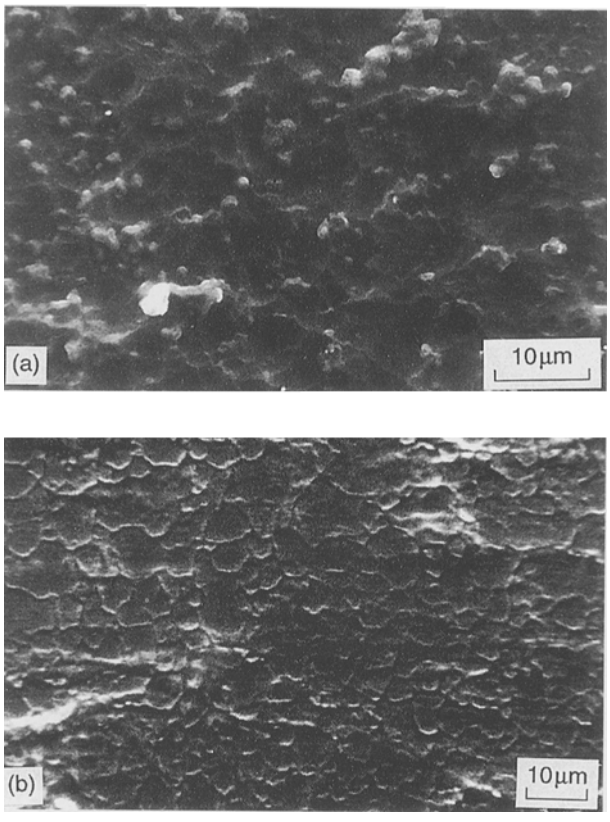

Figure 4 Scanning electron micrographs of as-prepared (a) specimen Ti–AsP and (b) specimen St–AsP.

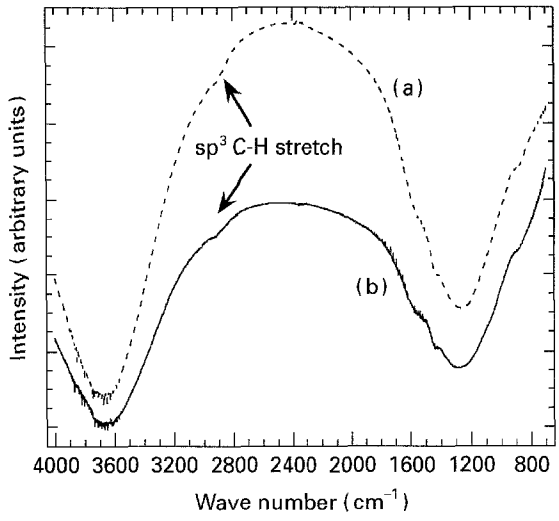

Figure 5 FTIR spectra from (a) specimen St–AsP and (b) specimen St60PBS4. These show the characteristic sp^3 C–H stretch around 2800 to 3000 cm^{-1}. There are no significant differences between the spectra (see Fig. 8).

TABLE III Surface roughness and coating refractive index data

Specimen code	Surface roughness R_a (μm)	Refractive index of coating
Uncoated steel	0.51 ± 0.08	-
St–AsP	0.54 ± 0.09	1.84 ± 0.16
St60PBS4	0.65 ± 0.08	1.85 ± 0.20
Uncoated titanium	0.35 ± 0.04	-
Ti–AsP	0.39 ± 0.03	2.34 ± 0.31
Ti37PBS4	0.45 ± 0.02	2.07 ± 0.23

3.2. Characterization of coatings

The FTIR spectrum of the St–AsP specimen shows characteristic sp^3-CH stretch peaks, visible as shoulders around 2900 cm^{-1} (Fig. 5). These peaks are relatively broad as a consequence of the strongly crosslinked structure of these DLC coatings. Similar features were observed in the FTIR spectrum of Ti–AsP. The refractive indices of the DLC coatings are presented in Table III. The refractive index of the coating on the steel substrate was slightly lower than that for the titanium, which may reflect a lower level of structural perfection. The surface roughness of the Ti–AsP was less than that of the St–AsP. This is attributable to the lower surface roughness of the titanium substrates. The coatings apparently reflect the substrate topography fairly closely. (In fact, the coated specimens have slightly greater roughness than the uncoated substrates, but the difference is not considered to be statistically significant.)

The Raman spectra of St60PBS4 and St–AsP show the characteristic D and G peaks of graphitic carbon, at 1357 and 1580 cm^{-1}, respectively (Fig. 6a and b). The Raman spectrum of the uncoated sample (Fig. 6c) reveals that all of the unidentified peaks in the spectra of specimens St60PBS4 and St-AsP are either from the substrate or are laser plasma lines.

The XPS spectrum of specimen St–AsP (Fig. 7a) indicates the presence of carbon and oxygen. There was no trace of silicon, either in elemental or combined form. One of the as-prepared samples was bombarded for 1 min by Ar^+ ions (at 3 kV acceleration voltage). The XPS spectrum of this sample showed

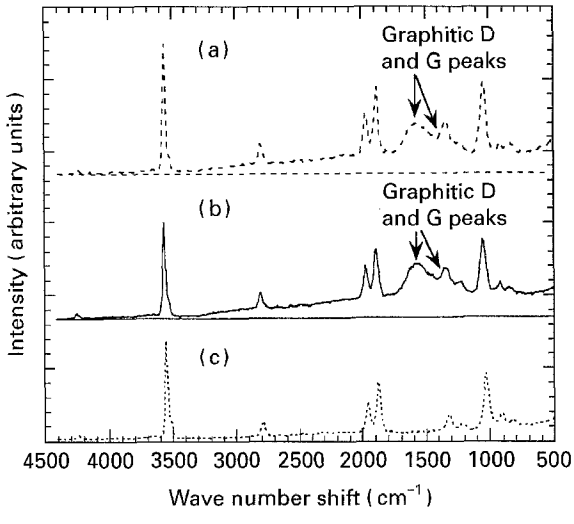

Figure 6 Raman spectra of (a) specimen St60PBS4, (b) specimen St–AsP and (c) an uncoated steel substrate.

a decreased oxygen peak and an increased carbon peak (Fig. 7b). This suggests that the oxygen was chemically bound at the surface of the coating. A narrow scan of the region where Si peaks would be expected (Fig. 7c) confirmed that silicon was not detected in these as-prepared samples.

All the above features were also observed in DLC-coated titanium samples. This indicates that the films on both the substrates were similar in terms of atomic structure and bond chemistry.

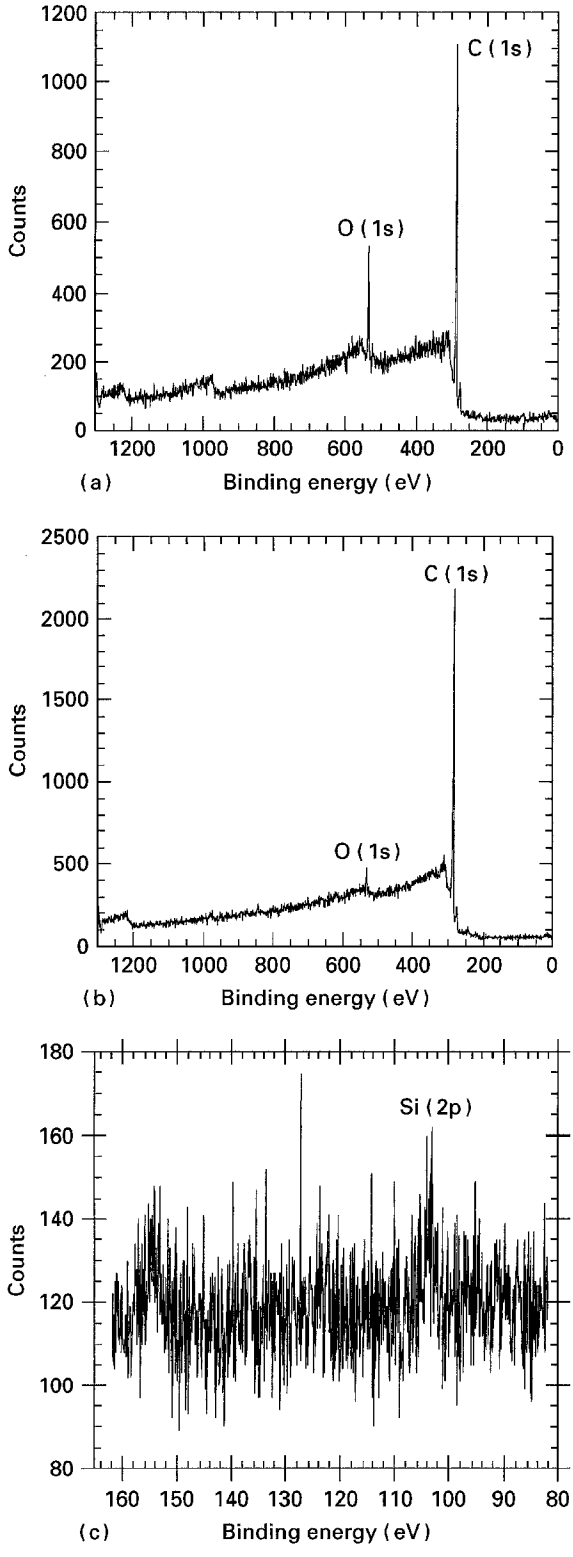

Figure 7 XPX spectra. (a) Broad scan of specimen St–AsP, (b) broad scan of specimen St–AsP after bombardment with Ar^+ ions for one minute and (c) narrow scan of St–AsP, in the range where any Si peaks would appear.

3.3. Effect of exposure on coating structure

The FTIR spectra of samples after exposure to fluids showed no significant difference from the as-prepared spectrum (Fig. 5). This is confirmed by Fig. 8, which shows a plot of the ratio of the FTIR signal from the St60PBS4 specimen to that from the St–AsP specimen, as a function of wave number. The plot is essentially flat, with no changes apparent near the C–C and

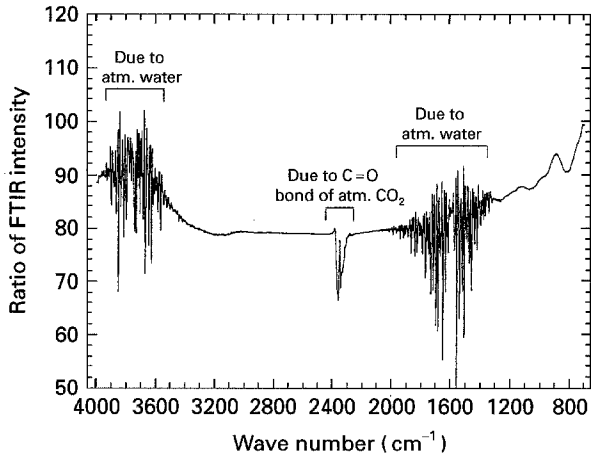

Figure 8 Ratio of the FTIR signal from specimen St60PBS4 (Fig. 6a) to that from specimen St–AsP (Fig. 6b). (The features at 2400 cm^{-1} and around 1600 and 3650 cm^{-1} are due to atmospheric CO_2 and H_2O, respectively.)

C–H vibration regions (3300 and 2900 cm^{-1}, respectively). The regions where differences are apparent (C=O stretch at 2400 cm^{-1} and bending modes of the H_2O molecule at 1600 and 3650 cm^{-1}) are a consequence of differences in levels of atmospheric CO_2 and water during the two scans. The slight increase of the baseline at the lower wave number end may be due to a slight variation in detector response for the two measurements. A comparison of Raman spectra from as-prepared and exposed samples also showed no significant change (Fig. 6). Similar behaviour was also observed for the coatings on titanium substrates. It can therefore be concluded that there were no significant changes in the atomic structure and bonding chemistry of the coatings during exposure to biological fluids.

The surface roughness of samples increased after exposure to PBS for 4 weeks, as a result of debonding of the coatings at several places (Table III). There was little change in the refractive indices of the coatings after exposure. (The difference in refractive index between the Ti–AsP and Ti37PBS4 is probably not significant.)

The XPS spectra of the samples after exposure to fluids were similar to the corresponding as-prepared samples, except in the case of specimens exposed to PBS, which showed clear silicon peaks. This is apparent in Fig. 9a, which shows a narrow scan for St37PBS4. This spectrum also shows a weak phosphorus 2p peak, which may be attributable to phosphate precipitates on the surface of the coating (also seen with SEM). The silicon peaks correspond to the 2s and 2p valence states. An expanded scan of the silicon 2p peaks, shown in Fig. 9b, revealed at least three distinct peaks. The binding energies of these peaks coincide with the 2p peaks of SiO_2, SiC and Si, their respective strengths being in that order [24, 25]. Since XPS is a surface analysis technique, sampling no more than a few nanometers, this indicates that the interfacial Si-rich layer must have been exposed. This suggests that the PBS solution reached the a-Si: H/a-C:H layer and attacked it. The sequence of events appears to be that the PBS solution penetrates to the

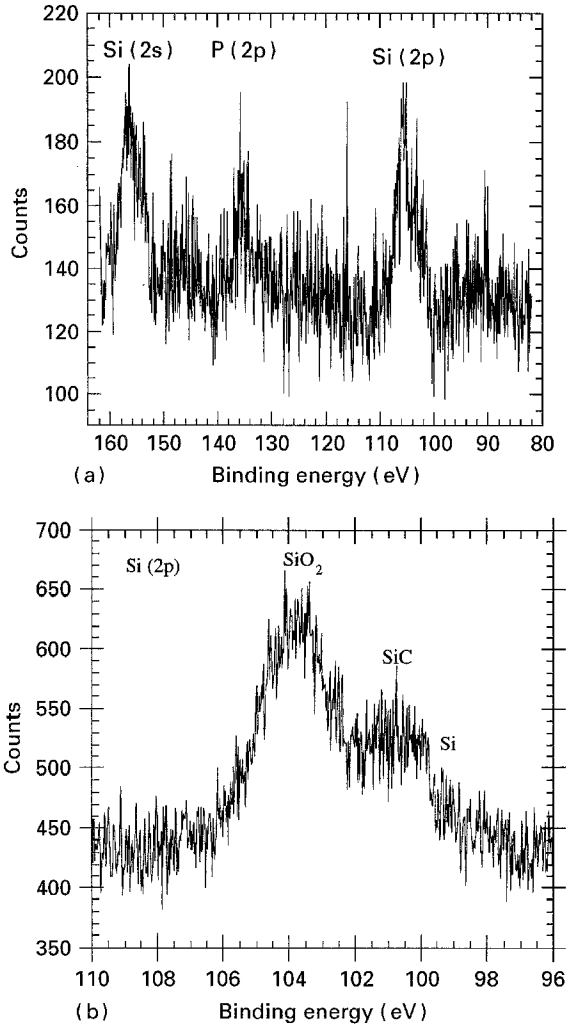

Figure 9 XPS spectra. (a) Narrow scan of specimen St37PBS4, (b) expanded narrow scan of specimen St37PBS4, showing the types of Si peak present.

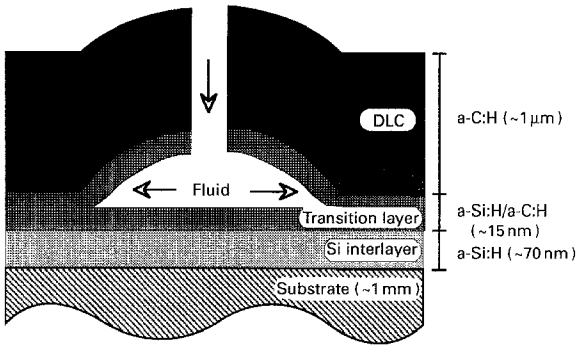

Figure 10 Schematic depiction of the proposed mechanism by which PBS fluid can cause damage and blister formation in DLC coatings.

a-Si:H/a-C:H interface, presumably through a surface perforation, then attacks the interface, causing the DLC film to debond and exposing the a-Si:H/a-C:H transition layer. This suggestion is depicted schematically in Fig. 10.

3.4. Effect of exposure on mechanical performance

The results of the adhesion measurements are shown in Table IV. Sets of parallel cracks appeared in all of the coatings at large substrate strains. The evolution of average crack spacing during straining of steel substrates is represented in Fig. 11. Saturation occurred at around 15% plastic strain. Straining was carried to well beyond this level for the measurement of saturation crack spacings. The coating tended to debond completely in areas with weak interfaces. This is apparent in the micrograph shown in Fig. 12. Such debonding was more widespread in samples exposed to PBS, particularly in those exposed at 60 °C. Parts of the coating in damaged areas became completely detached during the straining test and were lost before reaching the saturation crack distribution. In such cases, the true interfacial shear strength is considerably lower than that measured, since the debonded regions were ignored in the crack spacing estimation.

Even without taking account of such effects, the data presented in Table IV indicate that the saturation crack densities for steel samples exposed to PBS both at 37 °C and 60 °C, were significantly lower than for the as-prepared samples. This highlights the poorer adhesion of these films. The numerical values obtained for the interfacial shear strengths in Table IV are, however, potentially misleading, since the damaged films have very poor adhesion elsewhere. This localized poor adhesion clearly has serious implications in terms of the release of coating fragments during service.

For the titanium samples, the results of the substrate plastic straining test were similar to those on steel substrate. The fracture strength of films on Ti substrate was slightly lower, but the interfacial shear strength of the films was significantly higher, in agreement with earlier work [17]. Even though the microscopic examination did not show any significant damage of the film surface, the interfacial shear strengths of the coatings exposed to PBS were slightly lower than those of as-prepared specimens or those exposed to other fluids. This greater stability of coatings on titanium could have been at least partially a consequence of lower residual stresses in these coatings (which have a smaller thermal expansivity mismatch with the substrate than is the case for steel). Probably of more significance, however, is the generally lower level of defects in the films.

The results of the erosion tests are presented in Table V. These confirm the greater durability of films on Ti–6–4 substrates. It can be seen that the critical dose levels (and hence the erosion resistance) were significantly lower for the steel samples. These results also indicate that the erosion resistance fell on exposure to the fluids, particularly the PBS. These changes are not very large, but (as with the plastic straining experiments), it must be borne in mind that the damage due to exposure to fluids was severe, but localised. Tests like these, which probe large areas of the specimen, therefore tend to indicate only relatively modest degradation of adhesion and integrity. As for the adhesion testing, the results indicate that exposure of PBS did damage the coatings on the Ti substrates, but the effect was appreciably weaker than for those on the steel substrates.

TABLE IV Measured and deduced data concerning coating and interfacial strengths.

Specimen code	Average saturation spacing, $\bar{s}_\infty$ (μm)	Crack initiation strain, ε* (%)	Coating strength, σ* (= E_{coat} ε*) (GPa)	Saturation crack density ρ_∞ (mm^{-1})	Interfacial shear strength τ* (= $d\sigma^*\rho_\infty$) (GPa)
St–AsP	4.69	2.96	9.62	213	1.52
St37PBS4	5.12	2.92	9.49	195	1.37
St60PBS4	5.44	2.81	9.13	184	1.25
St37SER4	4.78	2.94	9.55	209	1.47
St37WAT4	4.54	2.97	9.65	220	1.57
Ti–AsP	2.68	4.53	8.07	373	3.74
Ti37PBS4	2.84	4.43	7.88	352	3.46
Ti37SER4	2.72	4.50	8.01	368	3.68
Ti37WAT4	2.62	4.47	7.95	381	3.77

(E_{coat} = 220 GPa (on steel) and 185 GPa (on Ti–6–4), d, (film thickness) = 1.1 μm (on steel) and 1.2 μm (on Ti–6–4)

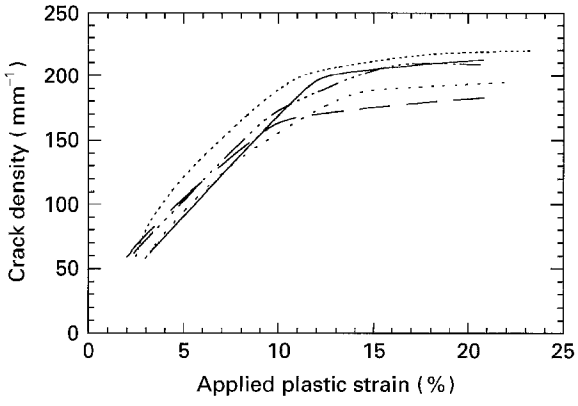

Figure 11 Variation of average crack density with applied plastic strain. The saturation crack density for the sample exposed to PBS at 60 °C is significantly lower than those for the other samples (---- St37WAT4, – – – St37SER4; - - - St37PBS4, — · — St60PBS4; —— ST–AsR).

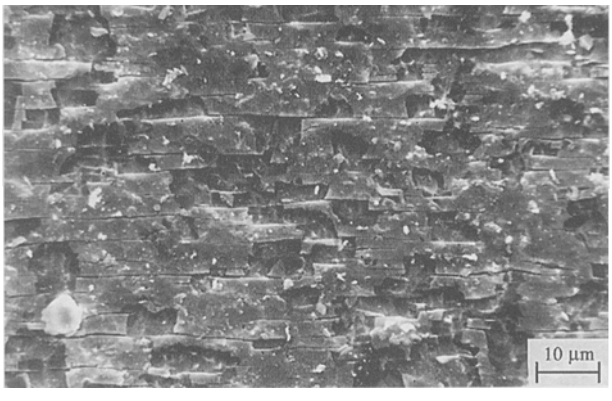

Figure 12 Scanning electron micrograph of specimen St30PBS4 after the substrate plastic straining test, showing delamination of areas with weak interfaces.

4. Conclusions

Diamond-like carbon coatings on stainless steel and titanium substrates have been exposed to different biological fluids, in order to examine the effect of this exposure on the mechanical stability of the coatings.

In the as-prepared state, coatings on both substrates displayed excellent adhesion, particularly on titanium. Few obvious defects were apparent under scanning electron microscopy, although some small flaws could be detected. The incidence of these flaws in as-prepared samples was greater for the steel substrates.

TABLE V Erosion resistance of coatings, bombarded by a stream of silica particles at 5 kPa suction pressure. A high critical dose indicates good erosion resistance

Specimen code	Critical dose Q_c ($kg\,m^{-2}$)
St–AsP	18.5
St37PBS4	15.5
St60PBS4	13.5
St37SER4	17.9
St37WAT4	19.0
Ti–AsP	36.7
Ti37PBS4	32.1
Ti37SER4	35.4
Ti37WAT4	35.9

Some of the exposure trials led to marked, but localized, degradation and debonding of the coatings. This was particularly severe for the PBS fluid and was worse for the coatings on steel substrates. Water promoted little damage, while the serum (containing some PBS) was intermediate in effect. These localized areas of damage were clearly visible by SEM and also affected the response of the coatings to macroscopic testing of adhesion and erosion resistance.

The mechanism of damage of PBS appears to involve penetration of fluid through pre-existing small perforations or defects in the coating, followed by penetration along the interface between the DLC and a thin a-Si:H/a-C:H "bonding" layer between the DLC and the substrate. This has been supported by the SEM and XPS analysis. Damage and debonding of the coating became more widespread when the temperature of exposure was raised. This may be because the residual stress in the coating would be more tensile at higher temperature, encouraging fluid penetration. Alternatively, a lowering of fluid surface tension may have facilitated entry into smaller defects in the coating.

Coatings on Ti were clearly more resistant to damage than those on steel. This appears to be primarily a consequence of the coating having a higher integrity and lower incidence of flaws. It may, however, also be associated with stronger adhesion, perhaps a consequence of a localized reaction involving the bonding layer.

Acknowledgements

Financial support has been obtained from the Nehru Trust in India via the Cambridge Commonwealth Trust and the Overseas Research Award (LC), and from EPSRC (RB). Thanks are also due to Mr. A. Moss, of Cambridge University, for assistance with the XPS measurements and Dr D.R. Waterman, of Reading University, for help in sample preparation. Dr I.M. Hutchings, of Cambridge University, has given valuable assistance with the erosion measurements.

References

1. J. NARAYAN, W. D. FAN, R. J. NARAYAN, P. TEWARI and H. H. STADELMAIER *Mater. Sci. Eng.* **B25** (1994) 5.
2. J. C. PIVIN, *J. Mater. Sci.* **27** (1992) 6735.
3. E. I. TOCHITSKY, A. V. STANISHEVSKII, V. V. AKULICH, O. V. SELIFANOV and I. A. KAPUSTIN, *Surf. Coat. Technol.* **47** (1991) 792.
4. K. MIYOSHI, R. L. C. WU and A. GARSCADDEN, *ibid*, **54/55** (1992) 428.
5. T. L. PARKER, K. L. PARKER, I. R. McCOLL, D. M. GRANT and J. V. WOOD, *Diamond and Related Mater.* **3** (1994) 1120.
6. L. A. THOMSON, F. C. LAW, N. RUSHTON and J. FRANKS, *Biomaterials* **12** (1991) 37.
7. D. M. GRANT, I. R. McCOLL, M. A. GOLOZAR and J. V. WOOD *Diamond and Related Mater.* **1** (1992) 727.
8. A. H. LETTINGTON, *Phil. Trans. R. Soc. Lond. A* **342** (1993) 287.
9. E. MITURA, S. MITURA, P. NIEDZIELSKI, Z. HAS, R. WOLOWIEC, A. JAKUBOWSKI, J. SZMIDT, A. SOKOLOWSKA, P. LOUDA, J. MARCINIAK and B. KOCZY, *Diamond and Related Mater.* **3** (1994) 896.
10. A. OLBORSKA and M. SWIDER, *ibid.* **3** (1994) 899.
11. D. W. HOWIE and B. VERNO-ROBERTS, *Biomaterials* **9** (1988) 442.
12. D. W. HOWIE and B. VERNO-ROBERTS, *Clin. Ortho. Related Res.* **232** (1988) 244.
13. N. RUSHTON and T. RAE, *Biomaterials* **5** (1984) 352.
14. L. CHANDRA and T. W. CLYNE, in "New diamond and diamond-like films," edited by P. VINCENZINI (Techna Srl, 1995) pp. 299–306.
15. A. H. LETTINGTON, *SPIE* **915** (1988) 60.
16. A. -M. DURAND and K. ENKE, European Patent, EP 0 522 979 Al (1992).
17. L. CHANDRA and T. W. CLYNE, *Diamond Related Mater.* **3** (1994) 791.
18. D. C. AGRAWAL and R. RAJ, *Acta Metall.* **37** (1989) 1265.
19. P. H. SHIPWAY and I. M. HUTCHINGS, *Surf. Coat. Technol.*, **71** (1995) 1.
20. I. M. HUTCHINGS, in 2nd European Conference on Advanced Materials, Euromat'91 (1991) Cambridge, UK, T. W. Clyne and P. J. Withers (Eds.), Vol. 2, Institute of Metals, pp. 56–64.
21. P. H. SHIPWAY and I. M. HUTCHINGS, *Wear* **162–164** (1993) 148.
22. C. R. SEWARD, C. S. PICKLES, R. MARRAH and J. E. FIELD, in "Window and dome technologies and materials III (San Diego, 1992) pp. 606–611.
23. J. E. FIELD, E. NICHOLSON, C. R. SEWARD and Z. FENG, *Phil. Trans. R. Soc. Lond. A* **342** (1993) 261.
24. P. SANDER, U. KAISER, M. ALTEBOCKWINKEL, L. WIEDMANN, A. BENNINGHOVEN, R.E. SAH, and P. KOIDL, *J. Vac. Sci. Technol.* **A5** (1987) 1470.
25. P. SANDER, L. WIEDMANN, A. BENNINGHOVEN and R. E. SAH, in E-MRS Meeting (1987), Vol. XVII, MRS, pp. 305–311.

Received 17 November 1994
and accepted 27 March 1995